Free-standing open space microfluidic devices by dry resist lamination

Downloaded from: https://research.chalmers.se, 2026-10-15 05:32 UTC

Citation for the original published paper (version of record):
Liu, R., Pedrueza Villalmanzo, E., Fatima, F. et al (2025). Free-standing open space microfluidic devices by dry resist lamination. Microfluidics and Nanofluidics, 29(7).
http://dx.doi.org/10.1007/s10404-025-02818-3

N.B. When citing this work, cite the original published paper.

research.chalmers.se offers the possibility of retrieving research publications produced at Chalmers University of Technology. It covers all kind of research output: articles, dissertations, conference papers, reports etc. since 2004. research.chalmers.se is administrated and maintained by Chalmers Library

(article starts on next page)

Microfluidics and Nanofluidics (2025) 29:47
https://doi.org/10.1007/s10404-025-02818-3

RESEARCH

Free-standing open space microfluidic devices by dry resist lamination

Rui Liu[1] · **Esteban Pedrueza-Villalmanzo**[1] · **Farah Fatima**[1] · **Aldo Jesorka**[1]

Received: 18 March 2025 / Accepted: 20 May 2025
© The Author(s) 2025

Abstract
We present a cleanroom-compatible fabrication route to open space microfluidic devices, utilizing a multilayer lamination/photolithography process on the wafer scale. The devices were applied to generate and maintain molecular surfactant films. In a dedicated setup, film stability was investigated in conjunction with 108 kHz ultrasonic sound, and response to acoustic waves in the audible range was determined.

Keywords Lamination · Thin surfactant films · Open space · Dry film photoresist

Abbreviations

USS	Ultrasonic sound
QDR	Quick drain rinse
BOE	Buffered oxide etch
PVD	Physical vapor deposition
PET	Polyethylene terephthalate
PEB	Post exposure bake
CTE	Coefficient of thermal expansion

1 Introduction

Microfluidic technology has found a solid place in many areas of research, product development and industrial production. Apart from diagnostics (Gervais et al. 2011), drug delivery (Liu et al. 2017), and analytical chemistry (Ohno et al. 2008), which constitute the main areas of use of microfluidic chip technology today, technical areas such as ink jet printing and micro cooling are a significant part of scientific research and industrial application environments. Open space or open volume microfluidics is a sub-field of channel-based microfluidics, which features devices with channels exiting at the periphery of the device. This allows for exposure or superfusion of objects outside the chip boundaries, such that fluidic flows are dispensed over external objects on the microscale. It is often beneficial if objects of interest do not need to be enclosed in chip-internal space. Commercial applications for use in cell biology research already exist (Ainla et al. 2012a). Localized and single cell superfusion in tissue cultures (Ainla et al. 2012b; Ahemaiti et al. 2013) as well bioprinting (Jeffries et al. 2020) are among the successfully targeted application areas.

In our previous work we developed a fabrication process for free-standing, layered SU-8 microfluidic probes, employing a negative photoresist process. However, the fabrication was laborious due to the use of liquid photoresist, unconventional lift-off layers and the need for bonding of the fabricated layers (Kim et al. 2017). A more capable and simplified fabrication approach addressing the challenges inherent in this route was necessary to enable reliable high-yield production. Major benefits of hard polymer devices are organic solvent compatibility, the small footprint of the channel exit area, optical transparency and the ability to implement printed metal structures, e.g. electrodes or sensors within the devices (Paredes et al. 2015; McIntyre et al. 2020).

We have now investigated dry negative photoresist sheets in conjunction with a multilayer lamination process. Dry film photoresist has widespread use in printed circuit board technology (Maurischat 1998). It is an epoxy material which is in its process properties comparable to the liquid SU-8 resist formulation. By means of lamination equipment it can be stepwise deposited to obtain multilayer assemblies

✉ Rui Liu
rui.liu@chalmers.se

Aldo Jesorka
aldo.jesorka@gomod.eu

[1] Department of Chemistry and Chemical Engineering, Chalmers University of Technology, Göteborg 412 96, Sweden

Published online: 23 June 2025

where each layer is individually photolithographically patterned on the same substrate. Pre-defined film thickness ensures that device features are highly homogenous across even large wafers; solvent and resin waste are reduced. Spin-coating, long wafer rest periods, soft bake and bonding steps are eliminated (Roos et al. 2022). Although the unit cost of dry resist sheets is relatively high for small quantities, a cost reduction can be expected when projected onto potential commercial use scenarios.

Dry film photoresist has earlier been used to fabricate millimeter wave waveguide components (Farjana et al. 2021), single and multilayer molds (Koucherian et al. 2022) and masters for microfluidic devices (Mukherjee et al. 2019). Direct fabrication of microfluidic devices was also achieved, although only on solid carrier substrates (Roos et al. 2022).

Free-standing devices made by this technology have thus far not yet been reported, which prompted our investigation into the feasibility of the dry resist route, targeting a particular open space application. We show a robust fabrication process using a SiO_2 sacrificial layer and report essential details regarding alignment strategy, lamination parameters, lift-off conditions, critical process problems and application examples.

We applied our fabrication strategy in an "acoustic soap film lab-on-a-chip" to develop a dedicated open space design for application in interface science, intended to semi-automatically create surfactant (soap) films on the millimeter to submillimeter scale and control the film parameters through microfluidic flow for investigations of film properties, integrated in a 3D-printed platform for facile characterization of surfactants in solution. Besides providing a suitable interface to optical microscopes and semiautomatic film formation, our foremost interest was the stabilization of soap films in this platform, such that manipulation of the films for characterization and utilization is efficiently possible over extended periods of time.

Acoustic waves have shown to prolong the lifetime of a soap film of comparable diameter (Ng et al. 2020), which established a practically useful time window for interacting with the film to conduct measurements and manipulation. Ng et al. investigated in detail the effects of audible sound frequencies, although at unpleasantly high intensities > 107 dB (Ng et al. 2020). We combined our microfluidic chip device with an ultrasonic sound (USS) resonator operating at 108 kHz/1.5 W and were able to attain similar stabilization results, but in an inaudible manner. By simultaneously exposing the films to moderately intense acoustic waves between 1 and 4 kHz at ~35 dB sound level, we could distinguish two modes of film response: droplet ejection and acoustically induced film rotation accompanied by vortex formation. The latter was also reported by Ng et al. (Ng et al. 2020), although in a different frequency range between 9 and 18 kHz.

2 Methods

2.1 Microfabrication

2.1.1 SUEX free-standing open space microfluidic devices

Fabrication of SUEX devices was performed in the Nanofabrication Laboratory at MC2, Chalmers University of Technology. All chemicals and solvents used were of high purity electronic grade, which were provided by the cleanroom facility.

A prototype process was developed on the 2" wafer scale, using double-side polished Si wafers (Ø 2", n-type < 100>, thickness 280 ± 10 µm, MicroChemicals GmbH, Germany).

2.1.1.1 Wafer preparation The wafer was cleaned in acetone for 3 min using an ultrasonicator, thereafter QDR-rinsed and blow dried. The wafer was placed into buffered oxide etch (BOE) solution (7:1 ammonium fluoride: hydrofluoric acid) for 5 s, QDR-rinsed, and blow-dried. The wafer was baked at 130 °C for 3 min and cooled down on a metal plate.

2.1.1.2 Backside alignment marks Hexamethyl disilazane (HMDS, Stangl) vapor was applied for 1 min at 100 °C to the cleaned wafer. Microposit S1813 positive photoresist (Shipley) was spin-coated onto the wafer (60 s / 4500 rpm / acc 2000), according to the manufacturer recommended process to get ~ 1.3 µm film thickness, following by a soft baking step (110 °C for 2 min) on a hotplate. Exposure was performed using a laser writer (MLA150, Heidelberg), wavelength 375 nm, dose 170 mJ/cm^2 and laser defocus level 2. The S1813 was developed in Microposit MF-CD 26 developer (Microresist Technology, Germany) for 1 min. The wafer was thereafter rinsed in water for 1 min, and blow-dried. Plasma ash was performed at 50W, 10 sccm O_2 for 30 s (BatchTop m/95, Plasmatherm). Thereafter, 40 nm chromium was PVD-deposited on the wafer (Evaporator PVD 225, Lesker) vacuum 5×10^{-7} Torr. A lift-off was performed in remover REM 400 (Microresist Technology, Germany) for 1 h. Double layer lift-off involving a dedicated lift-off polymer film below the resin can optionally be applied. This was found to be not necessary as the quality of the crosses was sufficient for marker detection. Further reduction of the lift-off time would not significantly shorten

the total process time. Finally, the wafer was washed with isopropyl alcohol, QDR-rinsed and blow dried.

2.1.1.3 Microfluidic devices Plasma ash was performed at 50W, 10 sccm O_2 for 30 s (BatchTop m/95, Plasmatherm) on the topside of wafer with backside marks. 200 nm SiO_2 was sputtered as a sacrificial layer (MS150 sputter, FHR). Another plasma ash was performed thereafter, preferably immediately before lamination.

The first layer was designed as the chip bottom layer. According to the manufacturers specification, the glossy polyethylene terephthalate (PET) coversheet was removed from 40 µm SUEX dry film (Microresist Technology, Germany). The film was laminated onto the SiO_2-coated wafer, using a common office laminator (PRO SERIES 3600, GBC) at a temperature of 65 °C, sheet transport speed 5 mm/s. The hazy PET coversheet of the SUEX film, now located on top of the wafer laminate, was removed before the subsequent exposure step. Exposure was performed using a laser writer (MLA150, Heidelberg), λ = 375 nm, dose 9000–10,000 mJ/cm^2 and laser defocus level 4. Post exposure bake (PEB) was performed using a benchtop hotplate. The wafer was placed onto the hotplate under a thermo-isolating cover and heated from room temperature to 95 °C. The hotplate was then turned off to slowly cool down the wafer for 60 min until reaching room temperature. Extending this time can further reduce cracks. After PEB, the wafer was allowed to rest for an additional hour.

The second (middle) layer was designed as a channel layer, using a 75 µm SUEX dry film. The film was laminated on top of the laminated wafer at a temperature of 65 °C with a transfer speed of 5 mm/s. The hazy PET coversheet was removed and the wafer was exposed with a dose of 13,000 to 14,000 mJ/cm^2 and laser defocus level 6. PEB was performed as for the previous layer. The two layers of dry film were simultaneously developed for ~10–15 min in mr-Dev 600 (Microresist Technology, Germany), until the channel structures were free of unexposed resist.

The last layer was designed as the roof layer, featuring well openings for channel access. The glossy PET coversheet was removed from 40 µm SUEX dry film. The film was laminated on top of the laminated wafer at a temperature of 70 °C, transfer speed 35 mm/s. The last layer requires faster transfer in order to avoid the collapse of the channel ceilings at the exits. The hazy PET coversheet was again removed. and the layer was exposed with a dose of 9000–10,000 mJ/cm^2 and laser defocus level 4. PEB was performed in the same way as described for the previous layers. The wafer was again developed with mr-Dev 600 developer for ~5 min for development of the chip devices, using vigorous spray development with a strong fluid stream by means of a spray bottle. The critical importance of this step for laminated open channel devices is discussed in detail in a subsequent section. Final lift-off was thereafter performed in BOE. The microdevices were collected, rinsed copiously with water to completely remove the acidic lift-off solution, blow dried and packaged.

2.2 Device characterization

2.2.1 Flow rate determination

The flow rate was determined by measuring the mass of a water droplet produced at a pre-defined pressure controlled by an in-house developed pneumatic air pump. The flow rate was determined at 50, 60, 80, 100, 120, 160 and 200 mbar. Droplets of outflowing liquids were collected on a coverslip and their mass was determined on an analytical balance. The time necessary to generate a droplet was measured and the pressure/flow rate relationship was determined (cf. Fig. S1). Due to the large channel size and associated short time periods for droplet formation, evaporation loss was not considered. For 50 mbar pressure, the droplet formation time was only 6 min.

2.2.2 Pressure test to establish device and tape seal integrity

Pressure tests were performed on a freshly prepared device. Out of the 8 channels of equal length in the device, pressure test experiments were performed in the microfluidic device on three closed and open channels, respectively. Closed channels were prepared by sealing the open exits with epoxy glue, and the devices were mounted onto the resin printed interface block. The epoxy sealing of the channels is irreversible, thus renders the device unusable. Therefore, the fluidic experiments were performed on different devices. The compressed air was supplied through a needle reduction valve connected to a compressed laboratory air source of 6 bars. A digital manometer (PascoloEEx, Keller AG) was connected via a T-junction and the pressure on the channels was set to 2 bars. The pressure was maintained for ~20 s, then the air supply was turned off. The development of the pressure, i.e. leaking behavior, was recorded over time (cf. Figure 3 and Fig.S3).

2.3 Experimental set up

2.3.1 Chip holder setup for surfactant film observation

The setup consists of a film generation and observation chamber and a control unit (cf. Figure 4). The chamber

consists of three main parts, a bottom part which integrates the acoustics components, a middle part which integrates a mechanical arm to produce the surfactant film and holds the microfluidic chip interface block, and a top part with a glass window for stereo microscopy observation. The main parts were manufactured by 3D printing. Interfaces to functional components such as miniature speaker, 115 kHz USS resonator and servo arm were designed to fit according to the dimensions of the parts.

The control unit was also 3D printed using the PLA process and utilizes an ATMEGA2560 MCU along with common electronic parts. Firmware was produced using the Flowcode 8 development environment. Either a Prusa i3 MK3 printer and PLA filament or a Formlabs Form 3B+printer with Clear V4 resin were used for printing. Both printers produce generally equivalent components. The resin technology produces in contrast to the filament technology completely airtight parts, which is important e.g. for gas transfer studies. The control unit addresses three main functions: timing of the ultrasonic sound pulses, operation of a servo arm with a rubber wiper to generate/re-generate the surfactant film and the operation of an integrated peristaltic pump.

Ultrasonic sound pulses were generated using a generic ultrasonication resonator commonly applied in humidifiers (Philips, Ø 20 mm, 108 kHz, 1.5 W supply power).

Acoustic signals were produced using an audio sweep function generator set to unmodulated sine wave output without DC bias (Model 9205, Hung Chang, South Korea). Audio levels were roughly determined with a generic sound intensity meter (Acogedor 30–130 dB, China) at a distance of approximately 5 cm from the speaker at the wall of the lower base. We note that more accurate determinations require a dedicated sound laboratory with isolated walls.

2.3.2 Mounting of chip devices

Double-sided 2 mil adhesive transfer tape (3 M 467 MPF) was shaped to fit the chip device using a Explore 3 commercial blade cutter (Cricut, USA). The tape design matching the layout of the microfluidic device was created in AutoCAD and transferred to the cutter. The cut-out was performed using a standard fine point blade (cf. Fig. S4). The tape was first adhered to the chip device and thereafter to the interface block of the surfactant film investigation setup. Alignment of the tape vias to the chip wells and interface block openings were performed manually with sufficient accuracy.

2.3.3 Fluidics

Supply of fluids to the chip and flow control was performed using an external syringe pump (NE-1000, New Era Pump Systems) and a miniature peristaltic pump integrated into the control unit. An inflow was established with the syringe pump. The outflow rate was adjusted using the control unit in order to obtain the desired film size (cf. Figure 4D).

2.4 Surfactant film experiments

2.4.1 Fluidics

A 0.1% sodium dodecyl sulfate (Fischer Scientific) solution in MilliQ grade deionized water was used in all experiments.

2.4.2 Surfactant film formation

A total of 3 microfluidic devices were used in the experiments, excluding the devices used for pressure test and sectioning for channel dimension measurements. The interface block holding the microfluidic chip was inserted into the platform and connected to the pumps with flexible polymer tubing. Surfactant solution was pumped at 10–40 µL/min through one or more channels into the central open volume until the surface of the chip device became wetted around the circumference of the orifice. It is advantageous to use several channels coming from different directions at the same time, as suggested by our device design, since it facilitates rapid wetting of the entire open space boundary. The flow rate was then reduced to 1.7–2 µL/min, and the servo arm was actuated on the control unit, such that the rubber blade pushed the fluid across the central open space and produced a molecular surfactant film across it. Subsequently, the peristaltic pump was engaged to reduce the film thickness. A nearly equal inflow and outflow rate was set such that a constant flow is established around the film. Small adjustments were manually made to control the size of the meniscus at the open volume boundary. The ultrasonic resonator and acoustic signals were invoked as desired for film manipulation. SI video 1 shows the presence of a few small air bubbles at the periphery which were generated upon priming the chip. These bubbles can be aspirated into the outflow channel, but an influence of the bubbles on the film (film diameter, stability of film diameter in the central orifice) is not noticeable.

2.5 Microscopy

An Olympus MX50 microscope with 5x (numerical aperture (NA)=0.13) and 20x (NA=0.4) objectives were used to obtain images of the microfluidic device. The scale for the

images taken at 20x magnification was software-assigned to 2.94 pix/µm. Microscopy for film characterization and observation was performed using a Leica M205 FA stereo fluorescence microscope with a 1x objective.

3 Results and discussion

3.1 Device fabrication results

3.1.1 Process

Fabrication routes using photolithographically patterned thin negative photoresist layers as foundation for microfluidic devices have been reported in several earlier publications (Roos et al. 2022) as an alternative to SU-8 formulations. The use of liquid resin is limited as channel layers cannot be directly closed by a simple additional process step; alignment and bonding are required instead. Stepwise lamination of multiple dry photoresist films of very well-defined thickness offers an improvement. A channel layer can be easily closed by a roof layer, such that the fabrication process for a microfluidic chip device consists of only a simple series of lamination and photolithography operations (Fig. 1).

Successively, lamination and photolithography are applied layer by layer, as detailed in the method section. The first two layers (Fig. 1A and C) are individually exposed by a laser writer (Fig. 1B and D). They can be developed together (Fig. 1E), since the channel layer is located inside the device boundaries already defined in the bottom layer. The third layer (Fig. 1F) requires different lamination parameters. The speed is particularly relevant, as the top layer is to some extent squeezed into the sub-structure, as discussed in a later section. After laser writer exposure (Fig. 1G), development (Fig. 1H) and lift-off (Fig. 1I), the final device (Fig. 1J) is ready for use. Note that the center orifice of the top layer is 100 µm smaller in diameter (cf. Figure 1H-I), compared to the other two layers. This feature prevents distribution of surfactant solution on the top side of the chip during the filling step prior to film generation.

The initial silicon carrier wafer preparation steps are straightforward. Alignment marks were fabricated photolithographically on the back side, and a sacrificial layer was thereafter deposited. Chromium was used for the crosses, taking into consideration the acidic bath for the removal of the SiO_2 sacrificial layer, which the alignment marks need to endure, such that the carrier wafer can be reused.

The alignment marks are placed onto the bottom of the wafer. Top-side alignment has been also investigated, but locating and focusing on the alignment marks has proven to be difficult, especially for the topmost cover layer, which led to undesired misalignment (cf. Fig. S2). This problem might not be of large significance for a few very thin layers. Backside alignment produced excellent results regardless of layer thickness. It is noteworthy that double-side polished wafers need to be used to produce device-recognizable alignment marks on the back side.

For prototype development, the performance and flexibility of a laser writer is most suitable. However, laser intensities do not compare favorably with the UV mask aligner light sources. The process times are excessive due to the low resist sensitivity and take many hours already for a 4” wafer, depending on the layer thicknesses. This is the primary reason why a 2” wafer was used in our study. If the process has matured beyond the prototype phase, photomasks can be obtained for the individual layers and exposure times are reduced to a few minutes. However, the mask process faces similar marker recognition issues with the top layers, and backside alignment is also recommended.

The schematic blueprint and a photograph of the fabricated device are shown in Fig. 2A and B, respectively. The detailed view in Fig. 2C displays channel exits into the open volume, obtained after processing the last layer and release from the wafer, representative of the device shown in (A-B). Panel D shows a micrograph of the device after development of layers 1 and 2. Misalignment is negligible.

The design blueprints of the microfluidic devices need to be adapted to the peculiarities of the lamination process. Partial deformation and collapse of the roof layer in regions that have no direct structural support in the lower layers, e.g. wells, vias or channel exits into the open space, can be prevented with designed support structures. Supporting pillars were added close to the channel outlets and inlets in the vias. No roof deformation is visible on narrow channels (Fig. 2E). On wide channel exit geometries, which are advantageous to limit resist/developer aspiration during development, deformation of the roof still occurs, but not to the extent that the channels are blocked (Fig. 2F). Supports also prevent occasionally observed irregularities due to overexposure at the device periphery (Fig. 2G).

3.1.2 Lamination

The channel geometry is partially influenced by the lamination process. The different layers deviate slightly in the channel exit regions individually from their specified thicknesses (Fig. 2H). The bottom layer showed a measured thickness close to the defined 40 µm (within manufacturer specification), while the middle layer differs by 6.6% from the nominal layer thickness. The lamination compresses and merges the layers into each other. The first layer is largely unaffected, while the channel layer experiences compression. The red arrow in the figure points to the (designed) interface between two layers. The deviation from the

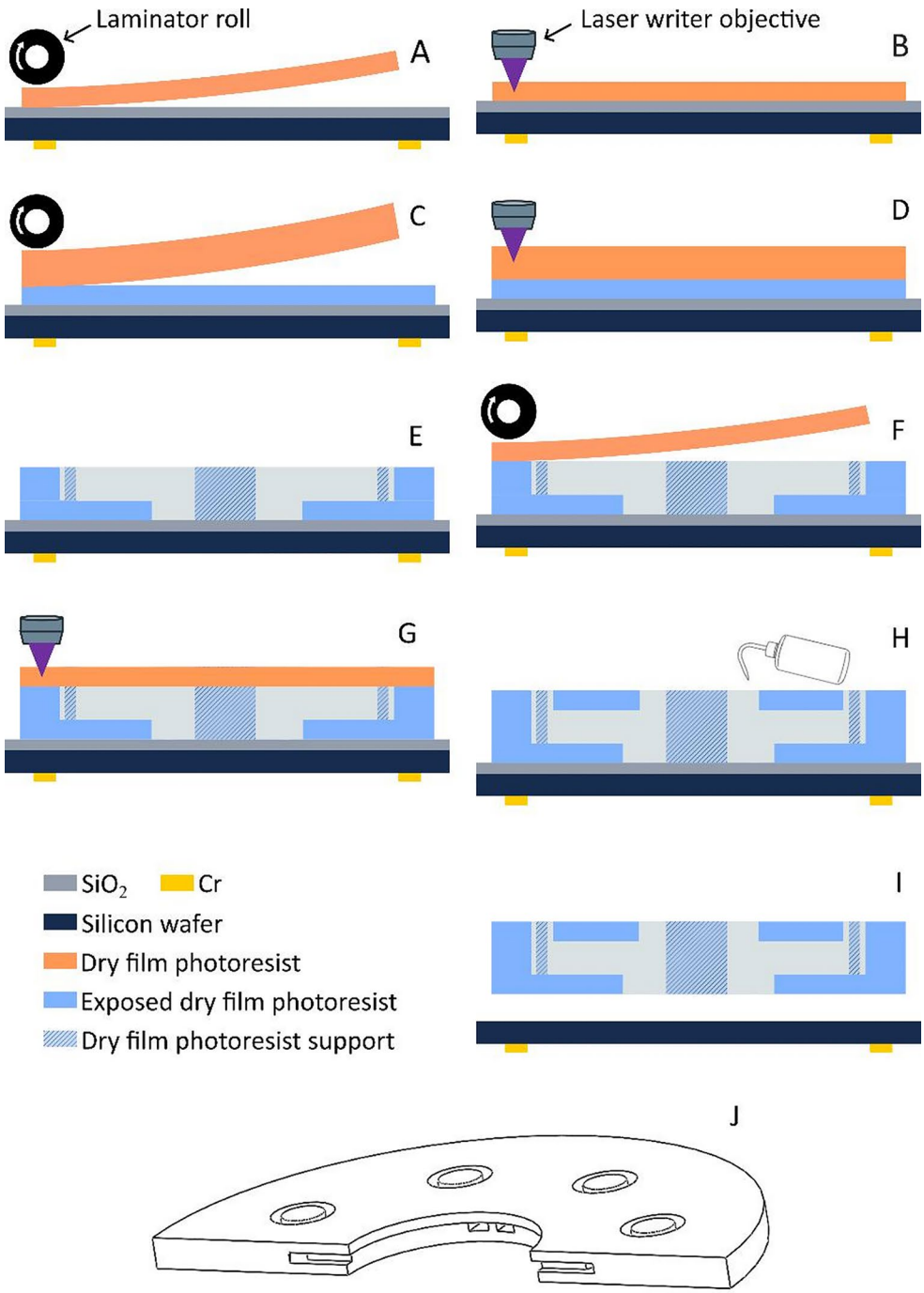

Fig. 1 Schematic illustration of the fabrication process of a SUEX free-standing open space microfluidic device (not to scale). (**A**) Laminating the first dry film photoresist. (**B**) Direct exposure by means of a laser writer. (**C**) Laminating the second dry film layer. (**D**) Laser writer exposure. Post-exposure baking follows each exposure step (not shown). (**E**) Joint development of the two post-baked dry films. (**F**) Laminating the third dry film layer onto the developed films. (**G**) Third laser writer exposure. (**H**) Spray development of post-baked film by means of a solvent spray bottle. (**I**) The lift-off of SUEX microfluidic device using BOE. (**J**) 3D section view of the final SUEX microfluidic device

designed dimensions should be taken into account when selecting sheet thicknesses with respect to a desired channel geometry and needs consideration in the process plan if the distance of the channel orifices from the device bottom is particularly important for its function.

Optimal lamination speed and temperature are slightly different for the individual layers. For the bottom layer located directly on the wafer and the intermediate layer, the lamination speed needs to be at 5 mm/s comparatively slow. This ensures sufficient contact to achieve strong adhesion to the substrate and, most importantly, between the laminate layers. Slow speed also prevents air inclusion between the layers. The third layer needs to be laminated at a much higher transfer speed, 35 mm/s was found to be optimal. Dry film partially softens at the lamination temperature, which can result in a collapse of the dry film roof into the channel structures. With fast lamination speed, this is prevented, but at the expense of having a larger amount of air bubbles entrapped. The adhesion strength between the top and channel layer does not appear to be negatively affected.

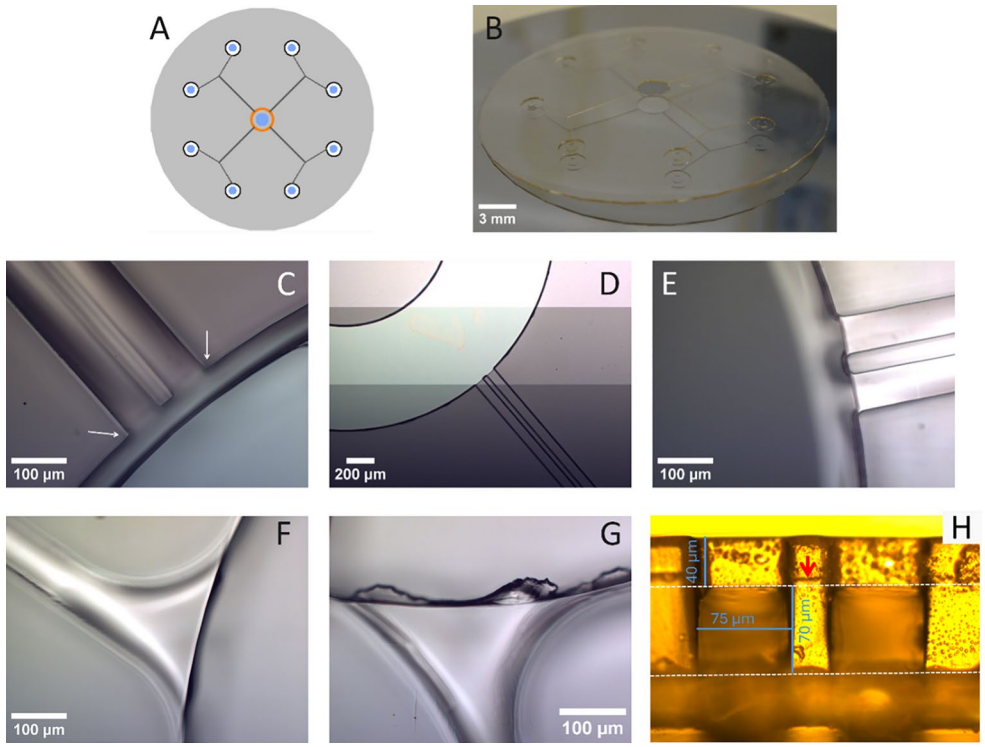

Fig. 2 (**A**) Schematic layout of the microfluidic chip design with channel exits into the open volume, along the boundary marked in orange. The device diameter is Ø 30 mm. The center orifice is Ø 3 mm and the eight radially symmetrical supply vias are Ø 1 mm. Structural support pillars inside the vias are highlighted in blue. (**B**) Photograph of the final free-standing device placed against a 2" silicon wafer background. The support pillars are visible in the vias. (**C**) Detail micrograph of two channel exits after the full three-layer process, viewed from the top side of the chip. The 50 µm top-side frame is in focus (cf. Figure 1H-J). The arrows point to the edge of the channel outlets. (**D**) Detail micrograph of the device after joint development of layers one and two, with no evidence of misalignment. Different brightness regions are due to the light conditions under the microscope. (**E**) Detail stereo micrograph of channel exits into the open space, viewed from the bottom side. The 50 µm top-side frame is not in focus. The channel roofs show no sign of deformation. (**F**) Micrograph of a channel inlet in a via, fabricated with support pillar. The channel inlet is deformed slightly but still open. (**G**) Top down micrograph of a channel inlet without support pillar. The collapsed roof can lead to overexposure artifacts. (**H**) Top down micrograph of the channel at the exit into the open space, viewed vertically through the channel. White dotted lines denote device layers. Blue solid lines represent measured dimensions. The red arrow points to the contact interface between two layers

This was confirmed by pressure test experiments. We note that the commercial laminator we used has certain limits: (i) the pressure cannot be adjusted; (ii) speed control has fixed steps; (iii) the distance between top and bottom roller cannot be readily adjusted without opening the instrument, which is prohibitive in shared environments. These are relatively minor issues and were not problematic for the designed channel/device structure and features in our process. However, they will have a critical impact on smaller features, e.g. channels smaller than 50 µm and thinner laminated layers.

A determination of flow rates through the device channels, assuming square channel geometry, gave an indication of the deviation from the design (cf. Tab. S1). Calculated vs. experimental results for two channels confirmed the reduction in channel cross section. The measured values of 8 ~ 9 nL $s^{-1}mbar^{-1}$, compared to the calculated values of 11 nL $s^{-1}mbar^{-1}$, amount to a deviation of 17–25%. A flow rate calculation was also performed on the measured dimensions of the device orifices (cf. Figure 2H), which we found in agreement with the measured flow rates.

3.1.3 Development

Development is uncritical for the first two layers. The manufacturer-recommended procedures for SU-8 resist are adequate. A particularly critical step in open space microfluidic device fabrication by dry lamination is the development process of the final cover layer. Unlike conventional devices with channels within the chip boundaries, open space chips have channel exits that are exposed to the developer solution in the development step. In contrast, conventional devices can be fabricated in a way that the roof layer seals all channels, vias and wells; they will become exposed to the surrounding fluid only during the release step at the end of the process. The unavoidable exposure of channel exits to the developer solution leads to difficulties. Upon dissolving, the dry resist of the top layer just above the channel exits

will at some point attain a consistency sufficient for flowing into the channels, driven by capillary forces. A viscous plug thus forms which is later difficult to displace. Seemingly obvious techniques such as sonication or extended development time typically led to more problems, namely crack formation and deformation of the devices. The problem is fortunately not prevalent on all device variants. In the large channels > 50 µm (lateral dimensions) that we have in the devices fabricated in our work, it is possible to wash out the resist plugs simply by means of a stream of fresh developer coming from a developer-filled spray bottle (cf. Figure 1H). A funnel-shaped design for the channel inlets in the vias also improves the situation. However, for much smaller channels than used in our device, the plug cannot be displaced by easy means. Higher pressure or a more sophisticated development strategy are needed. The fabrication of devices with smaller channels will be addressed in future work.

3.1.4 Lift-off

For the fabrication of free-standing microfluidic devices, release from the carrier substrate needs to be considered, i.e., a sacrificial layer is required. Although transfer tape was suggested earlier (Kim et al. 2017), unevenness due to unavoidable air inclusions reduces the quality of the devices and cancels the benefit of thin sheets with respect to uniformity. We therefore investigated conventional sacrificial layers, specifically a spin-on polymer (Omnicoat™) and SiO_2. OmniCoat™ was initially unsuccessfully used as a sacrificial layer. This confirms earlier reported poor adhesion with silicon and suggested that OmniCoat™ is not stable in SU-8 developer and only suitable for single layer SU-8 processes (Tatikonda et al. 2018). When OmniCoat™ was used as a sacrificial layer, SUEX was frequently fully or partially lifted off during the development of the last layer. To solve this issue, 200 nm SiO_2 was used as the sacrificial layer; standard BOE solution led to lift-off within 1 h (cf. Figure 1I). The carrier wafer could be reused after lift-off up to 4 times. Only cleaning and re-deposition of SiO_2 was required. Limiting is here the partial degradation of the Cr markers. This problem might be mitigated by using a different material for the crosses or by coating the back side with a thin fluoropolymer layer (Cytop, Telflon AF or similar).

3.1.5 Materials stress-cracks and wafer distortion

The coefficients of thermal expansion (CTE) of SU-8 and silicon are 50 ppm/K (Lorenz et al. 1998) and 2.5 ppm/K (Lang 1996) separately. The large CTE difference causes high residual stress and often leads to cracks in the microdevices (Abgrall et al. 2007). The formation of cracks can be, similarly to processing of SU-8, largely eliminated by a slow cool-down process after post exposure baking. Sharp corners in the channel structure were also avoided in our design. With too rapid cool-down, bowing of the carrier wafer can occur, which leads to vacuum problems during the exposure step. The problem of whole-wafer distortion was not consistently experienced and was prevalent largely on thin 2" wafers. When it occurred, a transparent sacrificial wafer (glass) was temporarily bonded to the back side by means of double-sided thermal release tape and removed after the exposure step. A thicker wafer or a different substrate material with a CTE close to SUEX (Abgrall et al. 2007) eliminates the problem altogether.

3.2 Device characterization results

3.2.1 Pressure test

Repeated pressure tests of a tape-mounted device with closed channels gave no indication of integrity loss over a time period of 20 s at 2 bars compressed air. This indicates that the lamination process produces robust channels of sufficient interlayer adhesion for intended use in the mbar pressure range. After turning off the air supply, the leaking behavior of the assembly was inspected, which shows in most cases a slightly increased loss rate due to small leaks in the supply lines. Since the test also affects the tape seal, this might be an indicator of a possible slow loss of integrity at high pressure, without affecting the intended operation of the device with supply pressures < 500 mbar (Fig. 3, cf. Fig. S3). When the test parameter was extended to 4 bars the bonding tape detached from the microdevice which itself remained intact (not shown).

3.3 Surfactant film experiments

3.3.1 Microfluidic surfactant film manipulation platform

The surfactant film manipulation platform was constructed in a modular fashion from 3D filament-printed components. Figure 4A shows a schematic drawing of the system with the mechanical arm to establish a film (Fig. 4B), and with dimensions suitable for application under a stereomicroscope (Fig. 4C-D). The total height of the device is 70 mm, of which 45 mm is the distance between USS resonator and mounted microfluidic device. The height can in principle be reduced to less than 40 mm, but the commercial low-cost resonator had a fixed operation power of 1.5 W, which required positioning at an appropriate distance to avoid unwanted disruption of the film. The controller was utilized to adjust USS pulse length and interval, control the outflow pump and actuate the servo arm to swipe over the chip device and produce the film. The integrated miniature

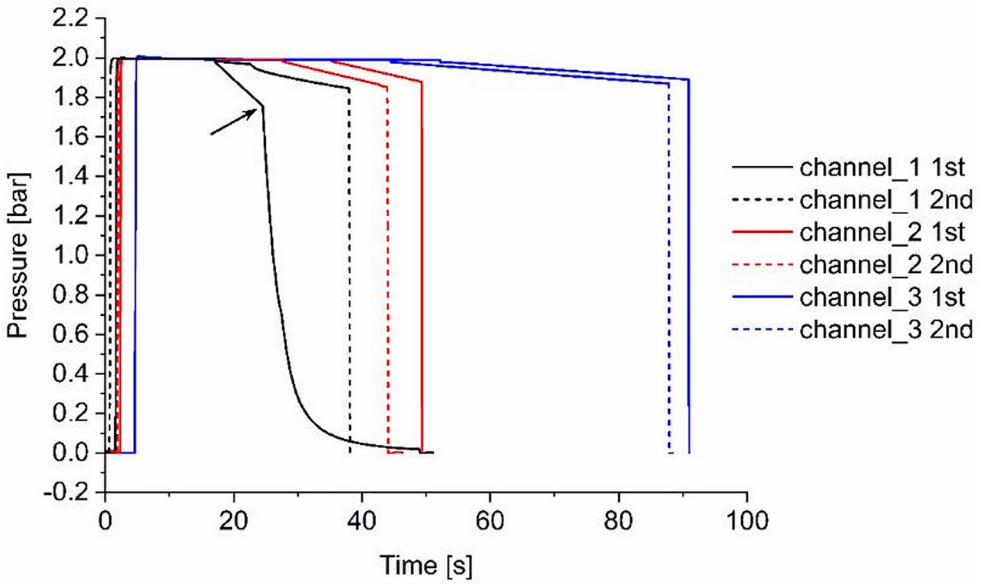

Fig. 3 Pressure tests repeated twice on 3 closed channels in the same sample chip, respectively. The channels were pressurized, then the compressed air supply was closed to reveal slow leakage. The arrow points to the time of full pressure release of channel 1

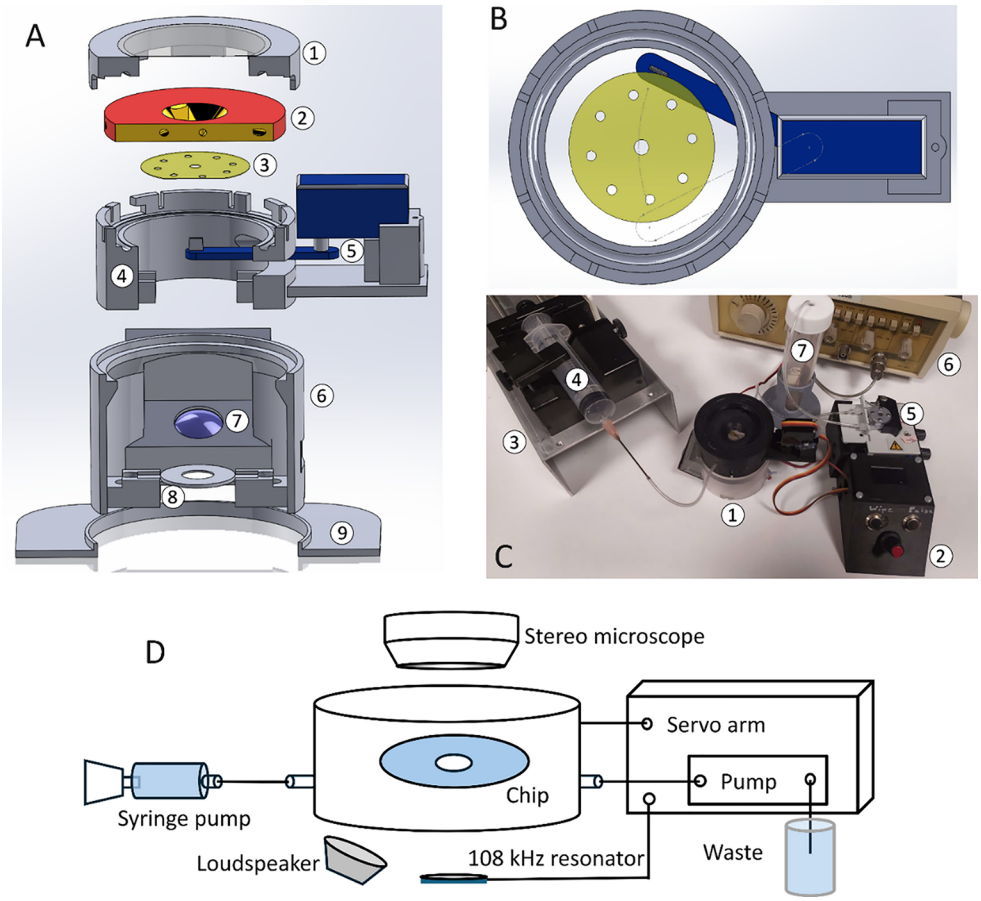

Fig. 4 Microfluidic surfactant film manipulation platform (not to scale). (**A**) Engineering drawing: (1) Top lid, (2) Interface block, (3) Microfluidic chip, (4) Upper base, (5) Servo arm, (6) Lower base, (7) Loudspeaker, (8) USS resonator, (9) Foundation. (**B**) Drawing of the servo arm for semiautomatic surfactant film formation. (**C**) Setup with (1) Platform, (2) Electronic controller, (3) Syringe pump/inflow, (4) Sample reservoir, (5) Peristaltic pump/outflow, (6) Frequency generator, (7) Reservoir outflow. (**D**) Schematic experimental setup for surfactant film

loudspeaker was supplied by an external sine wave generator with an adjustable output amplitude.

3.3.2 Film size control by microflow and stabilization of surfactant films by 108 kHz ultrasonic sound pulses and acoustic film manipulation

The assembled chip platform (Fig. 4A) was connected to fluid supply via pumps at the inlet and outlet (Fig. 4C). Initially, at an inflow rate of typically ~ 40 µL/min, the surfactant solution was pumped into the open space where a droplet formed, which by means of the mechanical arm (Fig. 4B) was transformed into a thin water-rich film spanning the central orifice. By balancing the in- and outflow at 1.7–2 µL/min, a soap film was produced in the center, which could be adjusted in size via control of the inflow/outflow ratio. The film size is subject to slow fluctuations which are manually compensated on either the in- or outflow side within ~ 1µL/min. The size fluctuations are a symptom of a hard-to-control imbalance between inflow and outflow. They are on a relatively long time scale and can be manually adjusted. Reprogramming the pumps on either in- or outflow is sufficient to counteract the imbalance. An electronic feedback loop controlled via real time image analysis could be used for automation in the future.

Figure 5A-C shows three different films sized from 0.5 mm (A) to 3 mm (C). Supporting Video S1 demonstrates the manual size adjustment process through change of pump parameters/flow rates, which can also be automated via a feedback system. Once the desired film size was attained, ultrasonic sound pulses of 300 ms length were applied periodically to the film, typically spaced 500–1500 ms, through the resonator located at the bottom of the setup (cf. Video S2). Despite continuous fluid flow around the film through the meniscus, water evaporation thins the film (Champougny et al. 2018; Pasquet et al. 2024), which is associated with a visible color change. Eventually a Newtonian black film results. At this point the film breaks which occurs within a few seconds after film formation. Acoustic sound waves superimpose rotational motion, typically intensity-dependent vortices and bulk film rotation (Ng et al. 2020). This mixes the thinning areas with fluid from the nearby environment, essentially repairing the local film inhomogeneities. Ultrasonic sound seemingly does not create strong

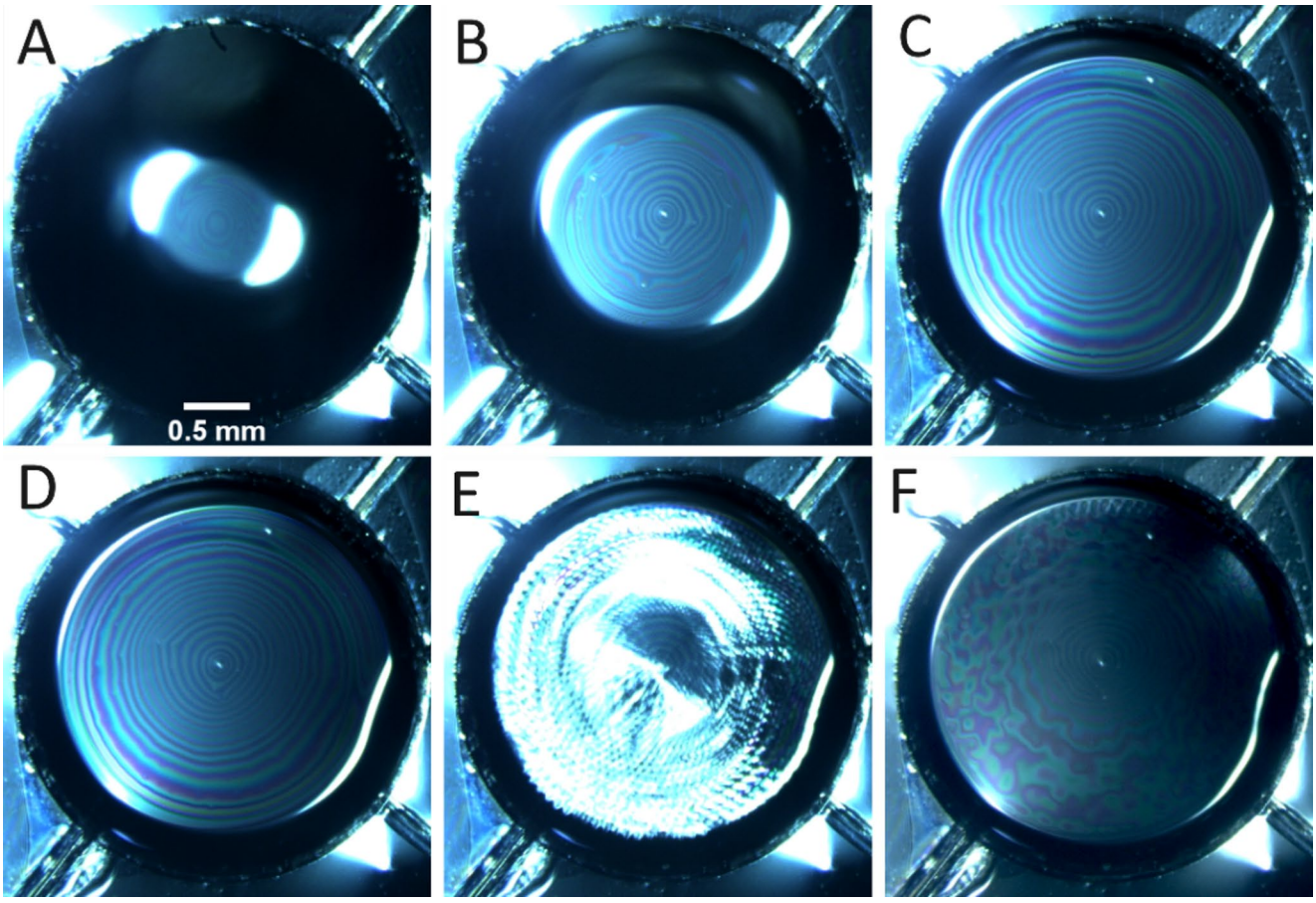

Fig. 5 (**A**) Micrograph of a soap film with radius ~ 500 µm formed in the center of the open space chip. (**B-C**) show micrographs of different soap film sizes by adjusting inflow/outflow ratio. (**D**) Micrograph of a newly formed soap film covering the entire open space area in the chip. (**E**) Micrograph of the soap film with a standing wave pattern at 108 kHz. (**F**) Micrograph of the soap film after USS pulse

rotational motion but causes transient standing waves which have a similar repairing effect. Figure 5D-F shows the impact of the pulses on a newly formed film (Fig. 5D); it visibly disrupts the film structure by redistributing fluid in the plane. The standing wave pattern (Fig. 5E) is weaker in the center of the film, recognizable by the difference in distortion of the colored concentric ring pattern originally produced during film formation (Fig. 5F). A pulse duration of 300 ms was found to be sufficient for the setup with the fixed power resonator used. An ultrasonic sound source with different power settings will certainly require adjustment of the pulse duration to be effective. The pulse was applied at intervals determined from the observed color changes in the film. It was adjusted such that a transition into blue/amber, corresponding to a film thickness of <250 nm, coincided with the onset of a new pulse. By this means, provided that fluid flow is continuously supplied around the film, soap films can be maintained for several minutes.

The application of an acoustic pulse pattern without supporting fluid flow was not sufficient to stabilize the films. Their lifetime did under these conditions not exceed a few seconds (cf. Video S3). Figure 6 shows a sequence of images taken over a time period of 9 s, during which the fluid-starved film destabilized and ruptured. While the first pulse at 1.5 s still caused adequate mixing (Fig. 6A-C), over the following 2.3 s the color change to blue/amber indicated rapid thinning (Fig. 6D). At 3.8 s edge thinning effects become visible. Since sufficient fluid is not provided through the microfluidic channels, fluid is no longer distributed into the film area. Therefore, thinning regions grow from the edge

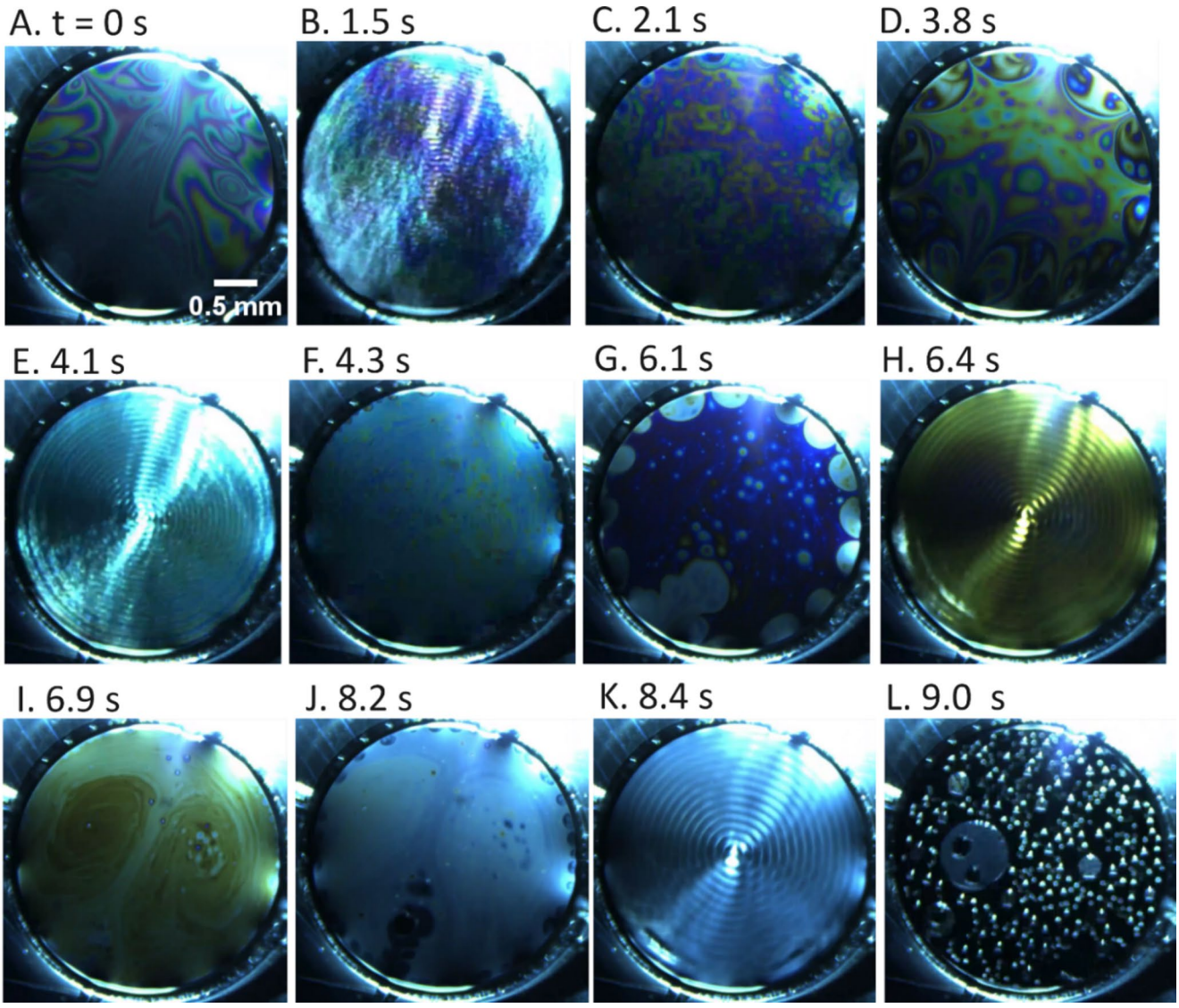

Fig. 6 Time series of the development of a surfactant film (0.1% SDS in H_2O) with USS resonator pulses under zero fluid flow conditions. Panel (**A**) shows a surfactant film formed in the microdevice, (**B**, **E**, **H**, **K**) USS resonator pulses, (**C**, **D**, **F**, **G**, **I**, **J**)film redistribution after pulses, and (**L**) 2D emulsion before film burst

towards the center. An additional pulse at 4.1 s was able to again repair the inhomogeneities (Fig. 6E-F). Scarce fluid inflow from the meniscus increased the thickness again, but inhomogeneous edge thinning increases (Fig. 6G). The next pulse redistributes the fluid again, but the amber color indicates thinning to ~150 nm over the entire area (Fig. 6H-I). The panel also shows that ultrasonic pulses do cause vortex formation, but at low intensity compared to audible frequencies. The film is subsequently invaded from the edges with black film pockets (Fig. 6J) (Exerowa et al. 1981). The final pulse (Fig. 6K) just before rupturing of the film causes a transformation that is reminiscent of an emulsion (Fig. 6L) (Seimiya and Seimiya 2021). This "2D emulsion" is characterized by numerous circular islands of varying diameter and increased thickness. The structure of these islands remains to be investigated. They are likely surfactant-containing microdroplets floating on the black film, which are formed by a spontaneous surface energy reduction mechanism related to the emulsification of immiscible fluids in bulk (Briscoe et al. 1999).

Audio frequencies supplied by a miniature speaker co-located in the lower frame were scanned over the range of 0 to ~20 kHz, and the response of the film was observed. Two distinct narrow frequency ranges were identified, in which the film showed unique responses. At 1 kHz and 35 dB sound intensity, the film displayed an increasing build-up of fluid in the center, which within seconds was ejected as a droplet (Fig. 7).

3.3.3 Droplet generation

The droplet generation process continuously repeated as long as fluid was supplied through the microfluidic channels. In order to record the droplet generation, the scaffold was oriented to 45 degrees from normal. During this process, the film was stabilized by periodic USS pulses of 300 ms length. Ng et al. have not observed this transport mode in their experiments, despite high acoustic intensities (Ng et al. 2020). A study by Drenckhan et al. shows droplet formation at the center of a suspended soap film upon excitation at 100 Hz acoustic frequency, and eventual ejection as a result of the competition between inertial forces and elastic restoring forces (Drenckhan et al. 2008). The system is characterized by a periodic change between Marangoni-type transport of fluid inwards due to the bending of the film at the peak of the sound wave and associated increase in tension at the center, followed by redistribution of the fluid when the film relaxes. Such flows in opposing direction typically lead to the generation of vortices. At the low frequency applied, the inwards flow apparently exceeds the backflow, possibly due to an increase in viscosity of the assembled fluid in the center. Collection and analysis of the expelled droplets could establish if the surfactant concentration is increased in comparison to the sample solution supplied. The color of the film around the droplet does not reveal any differences in thickness (cf. Video S4).

3.3.4 Film rotation and vortex formation

In the second audio frequency range at ~4 kHz, droplet generation and ejection were not observed. Instead, multiple vortices became visible (Fig. 8). The film started to rotate within the device orifice (cf. Video S5). This is generally in agreement with the main findings of Ng et al. (Ng et al. 2020), despite the large differences (18 kHz, 116 dB) in frequency and audio intensity in our study. The authors have shown a considerable change in film properties, visible by the increase of the number of vortices upon addition of 0.1 M NaCl to the surfactant solution. We have not investigated the influence of additives. The film integrity in our experiments was restored by means of periodic 300 ms ultrasonic pulses (Fig. 8D and H) in compensation for the much higher sound amplitude applied by Ng et al. (Ng et al. 2020) to stabilize their system. We also observed that the pulses tended to disrupt the rapid film rotation, which autonomously restarted each time after sonication ceased

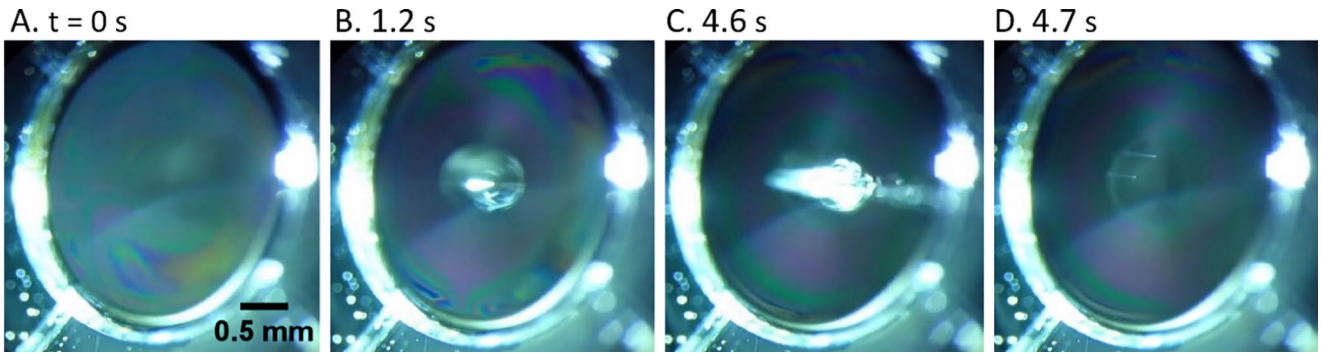

Fig. 7 Time series of liquid accumulation and droplet expulsion upon acoustic manipulation of a surfactant film (0.1% SDS in H_2O) with acoustic waves at 1 kHz/35 dB in the microfluidic device, supported by stabilizing ultrasonic sound pulses. Panel (**A**) shows the film at the beginning of the liquid accumulation, (**B**-**C**) the droplet generation, and (**D**) the film morphology immediately after expulsion

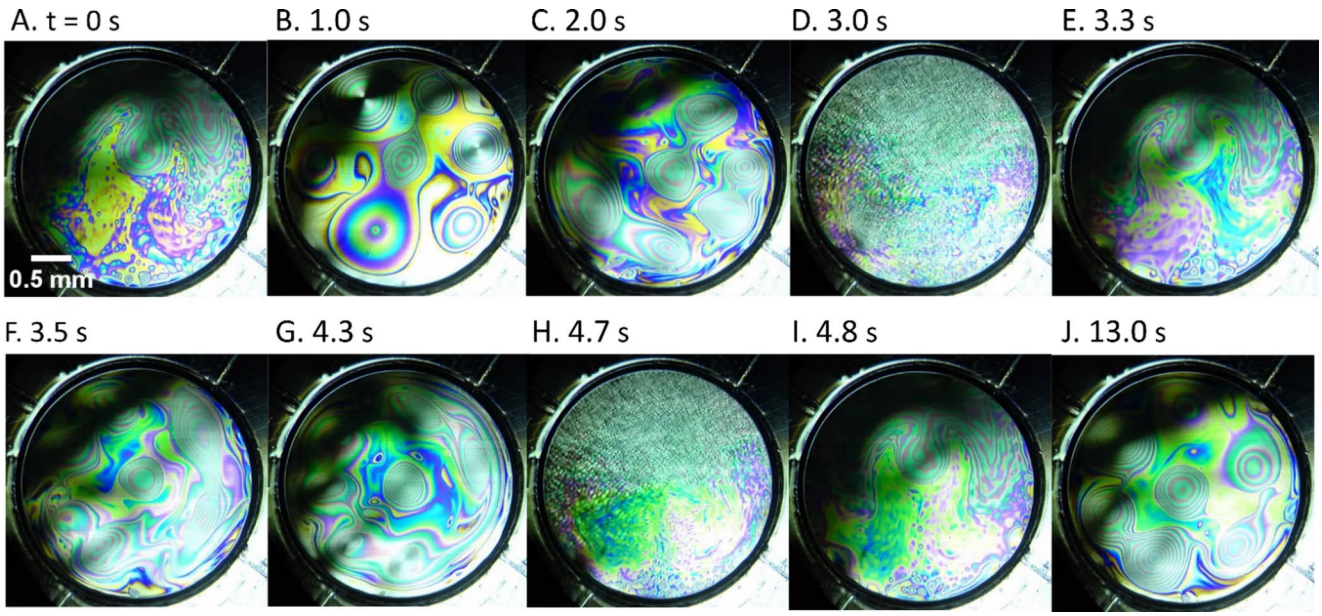

Fig. 8 Time series of surfactant film (0.1% SDS in H_2O) evolution upon acoustic manipulation at 4 kHz/35 dB in the microfluidic device with recurrent stabilizing ultrasonic sound pulses. The time series shows the formation of vortices, concurrent film rotation within the device orifice can be observed in Video S5. Panels (**D** and **H**) represent time points of ultrasonic sound pulse application

(cf. Video S5). We also note that the film thickness, apparent from the coloration visible in the images, is greater than in the reference study. Ng et al. discuss the various contributions to the film stabilization mechanism, particularly a pressure difference between the film and its border, capillary pressure, disjoining pressure and hydrodynamic pressure, with special reference to the importance of liquid flow in the film for acoustic waves to achieve stabilization (Ng et al. 2020; Nevolin 1984; Elias et al. 2017).

The existing studies on sound wave impact on soap film stability do not explicitly include the inaudible ultrasonic frequency range. Such detailed investigation is beyond the scope of our current investigation, which is more closely focused on the microfluidic device and its utility for studies of microscale soap films. Since we were only able to apply a fixed frequency, fixed intensity sound source to the surfactant system, more details on the dynamic properties of films of various compositions and exposure conditions are referred to future work.

4 Conclusion

A wafer-scale cleanroom compatible fabrication process using a multi-layer dry film negative photoresist process was developed and applied to successfully fabricate hard polymer free-standing open space microfluidic devices. This is, to our knowledge, the first report of the application of dry resist technology utilizing multi-layer lamination to fabricate free-standing open volume microfluidic chips on the wafer scale. The process has benefits in terms of simplicity and cleanroom instrument use, as compared to an earlier report from our laboratory where bonding equipment was used (Kim et al. 2017). Device fabrication, lamination parameters, resist development specifics, the choice of a sacrificial layer and other process-related details were reported, highlighting specific aspects of the process for the preparation of open space vs. closed channel devices. The fabrication process is satisfactory for channel size larger than ~50 µm. The microfluidic prototype devices were applied in a 3D-printed set-up suitable for the semi-automatic generation, manipulation and characterization of molecular surfactant films in combination with acoustic and ultrasonic sound frequencies. Our study is also the first report on the utilization of an open space microfluidic setup for surfactant film characterization with fluid flow control through microfluidic channels to form the film and achieve film diameter adjustment. Integration with peripheral components has shown to be uncomplicated, making microfluidic device use suitable for routine investigations of surfactant systems. On the application side, we documented our findings of film properties at different sound frequencies and established enhanced film stability through inaudible ultrasound pulses, which provides a less intrusive alternative to earlier reported stabilization strategies by means of high intensity audible sound. Due to its compactness and versatility, the described microfluidic setup can facilitate film characterization, for example by implementation of techniques for measurement of gas diffusion, electrochemical impedance and response to infrasound. Change of film composition to affect film stability

and thickness by means of fluidic flows is a possible future direction of investigation, where the properties of novel surfactants and mixing effects can also be evaluated. The application of the fabrication process to smaller channel sizes is a future goal of our multilayer lamination process development for open space devices, where a mask process for upscaling, reduced exposure time, further investigation of the discussed exit channel clogging phenomenon and improved sacrificial layer materials will be targeted.

Supplementary Information The online version contains supplementary material available at https://doi.org/10.1007/s10404-025-02818-3.

Acknowledgements We thank the engineers of the Microtechnology Center MC2 for their support. A.J. & R.L. acknowledge funding by the European Union's Horizon 2020 research and innovation programme under the Marie Skłodowska-Curie grant agreement No 956248. A.J., E.P.V., and F.F. acknowledge funding by the European Union's Horizon 2020 research and innovation programme under grant agreement No 899205.

Author contributions A.J. designed the study, generated the engineering designs and built the setup. R.L., E.P.V. and A.J. designed the microfluidic chips, R.L. and E.P.V. performed the device fabrication. A.J. and F.F. performed the surfactant experiments. R.L. characterized the devices. All authors contributed to data evaluation & analysis and contributed substantially to the manuscript.

Funding Open access funding provided by Chalmers University of Technology.

Data availability No datasets were generated or analysed during the current study.

Declarations

Competing interests The authors declare no competing interests.

Open Access This article is licensed under a Creative Commons Attribution 4.0 International License, which permits use, sharing, adaptation, distribution and reproduction in any medium or format, as long as you give appropriate credit to the original author(s) and the source, provide a link to the Creative Commons licence, and indicate if changes were made. The images or other third party material in this article are included in the article's Creative Commons licence, unless indicated otherwise in a credit line to the material. If material is not included in the article's Creative Commons licence and your intended use is not permitted by statutory regulation or exceeds the permitted use, you will need to obtain permission directly from the copyright holder. To view a copy of this licence, visit http://creativecommons.org/licenses/by/4.0/.

References

Abgrall P, Conedera V, Camon H, Gue AM, Nguyen NT (2007) SU-8 as a structural material for labs-on-chips and microelectromechanical systems. Electrophoresis 28:4539–4551. https://doi.org/10.1002/elps.200700333

Ahemaiti A, Ainla A, Jeffries GDM, Wigström H, Orwar O, Jesorka A, Jardemark K (2013) A multifunctional pipette for localized drug administration to brain slices. J Neurosci Methods 219:292–296. https://doi.org/10.1016/j.jneumeth.2013.08.012

Ainla A, Jeffries GDM, Brune R, Orwar O, Jesorka A (2012a) A multifunctional pipette. Lab Chip 12:1255–1261. https://doi.org/10.1039/C2LC20906C

Ainla A, Xu SJ, Sanchez N, Jeffries GDM, Jesorka A (2012b) Single-cell electroporation using a multifunctional pipette. Lab Chip 12:4605–4609. https://doi.org/10.1039/C2LC40563F

Briscoe BJ, Lawrence CJ, Mietus W, G P (1999) A review of immiscible fluid mixing. Adv Colloid Interface Sci 81:1–17. https://doi.org/10.1016/S0001-8686(99)00002-0

Champougny L, Miguet J, Henaff R, Restagno F, Boulogne F, Rio E (2018) Influence of evaporation on soap film rupture. Langmuir 34:3221–3227. https://doi.org/10.1021/acs.langmuir.7b04235

Drenckhan W, Dollet B, Hutzler S, Elias F (2008) Soap films under large-amplitude oscillations. Philo Mga Lett 88:669–677. https://doi.org/10.1080/09500830802220125

Elias F, Acharige SK, Rose L, Gay C, Leroy V, Derec C (2017) Vibration of soap films and plateau borders, as elementary blocks of a vibrating liquid foam. Colloids Surf A 534:85–93. https://doi.org/10.1016/j.colsurfa.2017.02.091

Exerowa D, Nikolov A, Zacharieva M (1981) Common black and Newton film formation. J Colloid Interface Sci 81:419–429. https://doi.org/10.1016/0021-9797(81)90424-0

Farjana S, Ghaderi M, Rahiminejad S, Haasl S, Enoksson P (2021) Dry film photoresist-based microfabrication: A new method to fabricate millimeter-wave waveguide components. Micromachines 12:260. https://doi.org/10.3390/mi12030260

Gervais L, de Rooij N, Delamarche E (2011) Microfluidic chips for Point-of-Care immunodiagnostics. Adv Mater 23:H151–H176. https://doi.org/10.1002/adma.201100464

Jeffries GD, Xu S, Lobovkina T, Kirejev V, Tusseau F, Gyllensten C, Singh AK, Karila P, Moll L, Orwar O (2020) 3D micro-organisation printing of mammalian cells to generate biological tissues. Sci Rep 10:19529. https://doi.org/10.1038/s41598-020-74191-w

Kim AA, Kustanovich K, Baratian D, Ainla A, Shaali M, Jeffries GDM, Jesorka A (2017) SU-8 free-standing microfluidic probes. Biomicrofluidics 11:014112. https://doi.org/10.1063/1.4975026

Koucherian NE, Yan SJ, Hui EE (2022) Fabrication of multilayer molds by dry film photoresist. Micromachines 13:1538. https://doi.org/10.3390/mi13101583

Lang W (1996) Silicon microstructuring technology. Mater Sci Eng R Rep 17:1–55. https://doi.org/10.1016/0927-796X(96)00190-8

Liu DF, Zhang HB, Fontana F, Hirvonen JT, Santos HA (2017) Microfluidic-assisted fabrication of carriers for controlled drug delivery. Lab Chip 17:1856–1883. https://doi.org/10.1039/C7LC00242D

Lorenz H, Laudon M, Renaud P (1998) Mechanical characterization of a new high-aspect-ratio near UV-photoresist. Microelectron Eng 42:371–374. https://doi.org/10.1016/S0167-9317(98)00086-0

Maurischat K (1998) Dry film photoresists-a never ending success story? Circuit World 24:34–37. https://doi.org/10.1108/03056129810198197

McIntyre D, Lashkaripour A, Densmore D (2020) Rapid and inexpensive microfluidic electrode integration with conductive ink. Lab Chip 20:3690–3695. https://doi.org/10.1039/D0LC00763C

Mukherjee P, Nebuloni F, Gao H, Zhou J, Papautsky I (2019) Rapid prototyping of soft lithography masters for microfluidic devices using dry film photoresist in a Non-Cleanroom setting. Micromachines 10:192. https://doi.org/10.3390/mi10030192

Nevolin V (1984) Parametric excitation of surface waves. J Eng Phys 47:1482–1494. https://doi.org/10.1007/BF00870072

Ng CY, Park H, Wang L (2020) Dynamic stabilization of foam films with acoustic sound. Langmuir 36:2966–2973. https://doi.org/10.1021/acs.langmuir.9b03767

Ohno K, Tachikawa K, Manz A (2008) Microfluidics: applications for analytical purposes in chemistry and biochemistry. Electrophoresis 29:4443–4453. https://doi.org/10.1002/elps.200800121

Paredes J, Fink KD, Novak R, Liepmann D (2015) Self-anchoring nickel microelectrodes for rapid fabrication of functional thermoplastic microfluidic prototypes. Sens Actuat B-Chem 216:263–270. https://doi.org/10.1016/j.snb.2015.04.041

Pasquet M, Boulogne F, Restagno F, Rio E (2024) Lifetime of vertical giant soap films: role of the relative humidity and film dimensions. Soft Matter 20:2374–2380. https://doi.org/10.1039/D3SM01629C

Roos MM, Winkler A, Nilsen M, Menzel SB, Strehle S (2022) Towards green 3D-Microfabrication of Bio-MEMS devices using ADEX dry film photoresists. Int J Pr Eng Man-Gt 9:43–57. https://doi.org/10.1007/s40684-021-00367-y

Seimiya T, Seimiya T (2021) Revisiting the Pearl string in draining soap bubble film first witnessed by Sir James Dewar some 100 years ago: A note of analyses for the phenomena with related findings. Phys Fluids 33:104102. https://doi.org/10.1063/5.0059830

Tatikonda A, Jokinen VP, Evard H, Franssila S (2018) Sacrificial layer technique for releasing metallized multilayer SU-8 devices. Micromachines 9:673. https://doi.org/10.3390/mi9120673

Publisher's note Springer Nature remains neutral with regard to jurisdictional claims in published maps and institutional affiliations.